

The (3+2) Neutrino Mass Spectrum and Double Chooz

Abhijit Bandyopadhyay^a and Sandhya Choubey^b

*Harish-Chandra Research Institute,
Chhatnag Road, Jhansi, Allahabad 211019, India*

ABSTRACT

The implications of extra sterile neutrinos for the Double Chooz experiment is expounded. The so-called “3+2” mass spectrum with 2 sterile neutrinos mixed with the active ones, is still allowed by the global neutrino data including MiniBooNE. We probe its impact on the resultant reactor antineutrino signal at the near and far detector of the Double Chooz experiment. The oscillations driven by the additional mass squared difference due to the sterile states bring an energy independent constant suppression at both the near and far detectors. We study to what extent the measurement of θ_{13} would get affected due to the presence of sterile mixing. We also give the projected sensitivity that Double Chooz will have to constrain the extra mixing angles associated with the sterile states.

^a email: abhi@mri.ernet.in

^b email: sandhya@mri.ernet.in

1 Introduction

Determining the mixing angle θ_{13} is the next priority in the field of neutrino oscillation physics. Discovery of a non-zero value for this mixing angle is a prerequisite for determining the two other ingredients of the neutrino mass matrix¹, *viz.*, the CP phase δ_{CP} and the sign of the atmospheric neutrino mass squared difference $sgn(\Delta m_{31}^2)$. Various experimental proposals have been put forward to resolve this perplexing issue and measure this hitherto unknown mixing angle. Accelerator based experiments such as T2K and NO ν A [1] involving conventional neutrino beams from pion decays are expected to come up in the near future. Superbeam upgrades of these facilities are also being envisaged. Pure ν_e and/or $\bar{\nu}_e$ fluxes from beta decay of highly accelerated radioactive ions stored in rings is called Betabeam and under ingenious experimental set-ups can give extremely good sensitivity to θ_{13} [2]. The ultimate neutrino oscillation machine of course would be the neutrino factory [3], which could provide unprecedented θ_{13} sensitivity, if indeed this mixing angle turns out to be extremely small. The main neutrino oscillation channel probed in these experiments are either the $\nu_\mu \rightarrow \nu_e$ conversion channel $P_{\mu e}$ or the $\nu_e \rightarrow \nu_\mu$ conversion channel $P_{e\mu}$, which is popularly known as the ‘‘Golden Channel’’. The conversion channels suffer from the intrinsic problem of parameter degeneracies, whereby one ends up with multiple fake solutions in addition to the true one. The three kinds of parameters degeneracies are the so-called $(\theta_{13}, \delta_{CP})$ intrinsic degeneracy [4], the $(sgn(\Delta m_{31}^2), \delta_{CP})$ degeneracy [5], and the $(\theta_{23}, \pi/2 - \theta_{23})$ degeneracy [6], and they together lead to a total eight-fold degeneracy [7] of parameter values.

The oscillation channel completely free of parameter degeneracies is the $\nu_e \rightarrow \nu_e$ survival channel, P_{ee} . This channel can be effectively probed in reactor based experiments. The crucial issue which needs to be addressed for maximum θ_{13} sensitivity is reducing the systematic uncertainties. It has been widely accepted that the best way of achieving this is by performing the experiment with two (or more) detector set-up. In these experiments a ‘‘near’’ detector is placed very close to the reactor cores and another one farther away, at the baseline optimal for observing near-maximal oscillations driven by Δm_{31}^2 [10]. Double Chooz [11, 12] is one such up-coming experiment which proposes to use the Chooz-B nuclear power plant in France. The other proposals that are being considered include ANGRA in Brazil [13], Daya Bay in China [14], and RENO in South Korea [15]. The first idea for using a near-far detector set-up in reactor experiments for measuring θ_{13} was put forth by the KR2DET collaboration in Russia [16]. However, this experiment was shelved due to various reasons. Two other very good proposals which were eventually turned down by funding agencies include the experimental proposal to use the Braidwood reactor in the U.S.A. [17] and KASKA in Japan [18].

There are two-fold advantage of the experimental set-up with reactor neutrinos. Firstly as mentioned above, these experiments use the P_{ee} channel, which is free from the problems of parameter degeneracies. Secondly, there are no problems of matter effects [19, 20, 21] in these experiments. However, there are at least two other experimental scenarios where very large matter effects in P_{ee} can be exploited to provide stringent tests of θ_{13} as well as $sgn(\Delta m_{31}^2)$. It has been realized that extremely large matter effects inside the supernova leaves an imprint on the resultant

¹The remaining unknowns, which include the absolute neutrino mass scale and the Majorana phases (if neutrinos are indeed Majorana particles) cannot be ascertained in neutrino oscillation experiments.

neutrino spectrum and hence in principle its possible to determine θ_{13} and $sgn(\Delta m_{31}^2)$ from the neutrino signal of a future galactic supernova [8, 9]. Very recently there has been a suggestion that in very long baseline experiments involving pure $\nu_e/\bar{\nu}_e$ fluxes such as Betabeams, one could effectively use the very large matter effects in P_{ee} to pin down θ_{13} and $sgn(\Delta m_{31}^2)$ [22].

The recent declaration of the MiniBooNE results [23] has brought back the issue of sterile neutrinos on the front line of neutrino physics. The MiniBooNE experiment was designed to test the oscillation claim of the LSND experiment [24]. Since the oscillation interpretation of the LSND signal demands a mass squared difference $\Delta m^2 \sim \text{eV}^2$, it cannot be accommodated along with the solar and atmospheric data within a three flavor framework. One therefore needs one or more extra neutrinos and these species necessarily must be sterile. For one extra sterile neutrino one would get the so-called 2+2 and 3+1 schemes [25]. Even before the MiniBooNE results, the 2+2 scheme was already disfavored from the solar and atmospheric data, while the 3+1 scheme suffered from severe tension between the LSND signal and the null results observed at other short baseline experiments [26]. However, all data could be fitted if one allows for 2 sterile neutrinos mixed with the active ones, leading to the so-called 3+2 mass schemes [9, 27, 28]. MiniBooNE has reported null signal in the energy range where it would have expected to see an excess of electron events if LSND experiment were due to two flavor oscillations. Though on the face of it this may look like a strong signal against the hypothesis of sterile neutrinos, in reality there is still ample room for their existence. For neutrino mass spectra with sterile neutrinos which predict $\Delta m^2 \sim \text{eV}^2$, one can see from the detailed analysis presented in [29] that even though the tension between the positive signal at LSND and negative signal at all other short baseline experiment including MiniBooNE, rules out the 3+1 scheme, the 3+2 scheme with 2 sterile neutrinos is still viable if one allows for CP violating phases. One should also keep in mind that even if it was proved that LSND was indeed wrong, it would only mean that sterile neutrinos in the eV^2 mass regime are ruled out. One could still envisage heavier sterile neutrinos which would have implications for astrophysics and cosmology, and these neutrinos could be mixed with active neutrino species.

In this paper we look at the implications of these extra sterile neutrinos for the Double Chooz experiment. For concreteness we work within the allowed framework of the 3+2 scheme which gives a viable explanation of current world neutrino data. However, our results can be easily extended to other scenarios since the oscillation driven by the extra Δm^2 corresponding to the sterile states anyway average out for the Double Chooz experiment. Our results can also be easily extended to the other reactor experiments mentioned before. We begin by discussing the oscillation probability in the 3+2 scheme in section 2. In section 3 we present the expected events in the near and far detector of Double Chooz if the 3+2 scheme was correct. Section 4 has our results with the full statistical analysis of the projected data set of Double Chooz. We end in section 5 with discussions and conclusions.

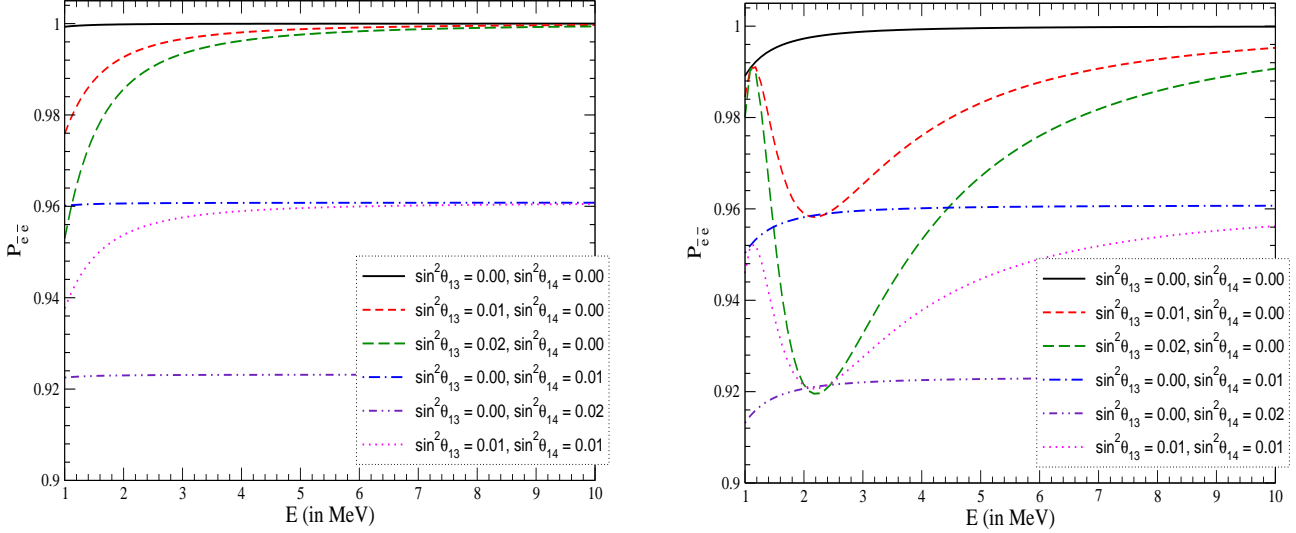


Figure 1: The $\bar{\nu}_e$ survival probability as a function of energy for the near (left panel) and far (right panel) detectors of Double Chooz. The 6 different line types are for 6 combinations of $\sin^2 \theta_{13}$ and $\sin^2 \theta_{14}$ which are shown in the panels. We assume that $\sin^2 \theta_{15} = \sin^2 \theta_{14}$.

2 Oscillation Probability in the 3+2 Scheme

The probability channel relevant for Double Chooz is $P_{\bar{e}\bar{e}}$ which for the 3+2 mass spectrum is given by²

$$P_{\bar{e}\bar{e}} = 1 - 4 \sum_{i>j} |U_{ei}^s|^2 |U_{ej}^s|^2 \sin^2 \left(\frac{\Delta m_{ij}^2 L}{4E} \right) - 4 \sum_{k>l} |U_{ek}^s|^2 |U_{el}^s|^2 \sin^2 \left(\frac{\Delta m_{kl}^2 L}{4E} \right), \quad (1)$$

where U^s is the mixing matrix and the indices i and j run from 1-3, l runs from 1-5 and k_s could be either 4 or 5. The oscillatory part of the third term of course will average out to $1/2$ for Double Chooz, reducing the probability to

$$P_{\bar{e}\bar{e}} = 1 - 4 \sum_{i>j} |U_{ei}^s|^2 |U_{ej}^s|^2 \sin^2 \left(\frac{\Delta m_{ij}^2 L}{4E} \right) - 2 \sum_{k>l} |U_{ek}^s|^2 |U_{el}^s|^2. \quad (2)$$

For the 3+2 mass spectrum we would have a 5×5 mixing matrix for which we choose the convention

$$U^s = R(\theta_{45})R(\theta_{35})R(\theta_{34})R(\theta_{25})R(\theta_{24})R(\theta_{15})R(\theta_{14})R(\theta_{23})R(\theta_{13})R(\theta_{12}), \quad (3)$$

²Note that for the Double Chooz experiment there are neither any matter effects nor any CP violating effect due the phases. The survival probability is therefore the same for neutrinos and antineutrinos.

where $R(\theta_{ij})$ are the rotation matrices and θ_{ij} the mixing angle. We do not show the CP phases in Eq. (3) for simplicity. The mixing matrix with the above convention is expressed as

$$U^s = \begin{pmatrix} c_{15}c_{14}c_{13}c_{12} & c_{15}c_{14}c_{13}s_{12} & c_{15}c_{14}s_{13} & c_{15}s_{14} & s_{15} \\ \cdot & \cdot & \cdot & \cdot & \cdot \\ \cdot & \cdot & \cdot & \cdot & \cdot \\ \cdot & \cdot & \cdot & \cdot & \cdot \\ \cdot & \cdot & \cdot & \cdot & \cdot \end{pmatrix}, \quad (4)$$

where $c_{ij} = \cos \theta_{ij}$, $s_{ij} = \sin \theta_{ij}$, and we show explicitly only the first row since the probability $P_{\bar{e}\bar{e}}$, involves only them. We can see that apart from the two usual mixing angles θ_{12} and θ_{13} which appear in $P_{\bar{e}\bar{e}}$ with standard three generation oscillations, we have 2 additional angles, θ_{14} and θ_{15} , which will affect the probability. If these mixing angles were zero, one would get back the $P_{\bar{e}\bar{e}}$ predicted by three generation oscillations. Of course for the energy and baseline of Double Chooz, the oscillations due to Δm_{21}^2 are extremely weak and as a result so is the dependence on θ_{12} . Therefore the dominant dependence of the probability would be on the mass squared difference Δm_{31}^2 and the mixing angles θ_{13} , θ_{14} and θ_{15} .

Current 3σ constraints [30] on the parameters driving the leading oscillations in solar [31], atmospheric [32], K2K [33], MINOS [34] and KamLAND [35] are

$$7.2 \times 10^{-5} \text{eV}^2 < \Delta m_{21}^2 < 9.2 \times 10^{-5} \text{eV}^2, \quad (5)$$

$$0.25 < \sin^2 \theta_{12} < 0.39, \quad (6)$$

$$2.0 \times 10^{-3} \text{eV}^2 < \Delta m_{31}^2 < 3.2 \times 10^{-3} \text{eV}^2, \quad (7)$$

$$\sin^2 2\theta_{23} > 0.9. \quad (8)$$

The best limit on the mixing angle θ_{13} comes from the combined constraints from global oscillation data including CHOOZ [36] and is given as [30]

$$\sin^2 \theta_{13} < 0.044. \quad (9)$$

The sterile sector receives constraints from the short baseline reactor and accelerator based experiments [26] which reported null signal, the LSND experiment [24] and MiniBooNE [23]. The best-fit values for the mass squared difference Δm_{41}^2 and Δm_{51}^2 are 0.87eV^2 and 1.91eV^2 respectively, if the low energy MiniBooNE data is also included [29]. The best-fit values for the elements U_{e4} and U_{e5} of the mixing matrix are 0.12 and 0.11 respectively [29]. Since in the convention adopted in this paper $U_{e5} = \sin \theta_{15}$ and $U_{e4} = \cos \theta_{15} \sin \theta_{14}$, this would translate to the best-fit values for the mixing angles as $\sin^2 \theta_{14} = 0.012$ and $\sin^2 \theta_{15} = 0.015$.

The Double Chooz experiment is being built to probe the mixing angle θ_{13} . However, since the probability depends also on the sterile mixing angles θ_{14} and θ_{15} , these angles also can be constrained in this experiment. The parameters Δm_{41}^2 and Δm_{51}^2 are of course averaged out and

hence cannot be probed, and as discussed before, the solar parameters Δm_{21}^2 and $\sin^2 \theta_{12}$ bring in a weak effect on $P_{\bar{e}\bar{e}}$. In what follows, we will keep Δm_{21}^2 and $\sin^2 \theta_{12}$ fixed at their best-fit values given in Eqs. (5) and (6). The true value of Δm_{31}^2 will be assumed to be $2.5 \times 10^{-3} \text{ eV}^2$ throughout. Also, *just for the sake of simplicity* we will take $\sin^2 \theta_{14} = \sin^2 \theta_{15}$ everywhere.

In Fig. 1 we show the probability $P_{\bar{e}\bar{e}}$ as a function of the antineutrino energy for 6 different choices of the mixing angles θ_{13} and θ_{14} . For all other oscillation parameters we stick to the assumptions mentioned in the previous paragraph. The left panel of the figure shows $P_{\bar{e}\bar{e}}$ at a distance of 280 m, which will be the average distance of the near detector from the 2 cores of the Chooz-B reactor. The right panel shows $P_{\bar{e}\bar{e}}$ for the far detector which will be at an average distance of 1.05 km from the 2 reactor cores. For the near detector, when $\theta_{14} = 0 = \theta_{15}$, we expect $P_{\bar{e}\bar{e}}$ to be almost 1 at high energies. However at lower energies, for $E \lesssim 4 \text{ MeV}$ there is a Δm_{31}^2 driven dip in the survival probability, the extent of the dip depending on the value of $\sin^2 2\theta_{13}$. When we put $\theta_{13} = 0$ and allow θ_{14} and θ_{15} to be non-zero, we get an energy independent suppression, depending on the value of these mixing angles. When all three mixing angles are non-zero we have an energy independent suppression driven by θ_{14} and θ_{15} superposed on the energy dependent dip at low energy due to θ_{13} . At the far detector the Δm_{31}^2 driven oscillations of course are absolutely pronounced and the amplitude of the oscillations are determined by the value of $\sin^2 2\theta_{13}$. The energy independent average oscillation due to the extra large mass squared differences due to the sterile states are superimposed on the standard oscillations. We can see from the figure that more than one combination of θ_{13} and θ_{14} (and θ_{15}) would give the same total suppression of the flux due to oscillations at the far detector. However, the shape of the resultant flux at the detector is expected to be different for the θ_{13} and θ_{14} (and θ_{15}) dependent oscillations.

3 Results

3.1 Number of Events at the Near and Far Detector

The Chooz-B reactor complex consists of two reactor cores, east (R_E) and west (R_W), with a total thermal power of 4.27 GW each. The $\bar{\nu}_e$ flux at the near (N) and far (F) detector can be written as

$$\Phi(E) = \frac{1}{4\pi L_{N,F}^2} \sum_i N_i^{fis} \phi_i(E) , \quad (10)$$

where $L_{N,F}$ is the distance from the reactor core to the near (N) or far (F) detector³, N_i^{fis} are the number of fissions per second for the isotope i in the reactor which we take from [37] and $\phi_i(E)$ gives the corresponding energy spectrum

$$\phi_i(E) = \exp \left(\sum_{k=0}^2 a_{ki} E^k \right) . \quad (11)$$

³The far detector is at a distance 1114.6 m and 997.9 m from R_E and R_W respectively, while the near detector is 290.7 m and 260.3 m away from them.

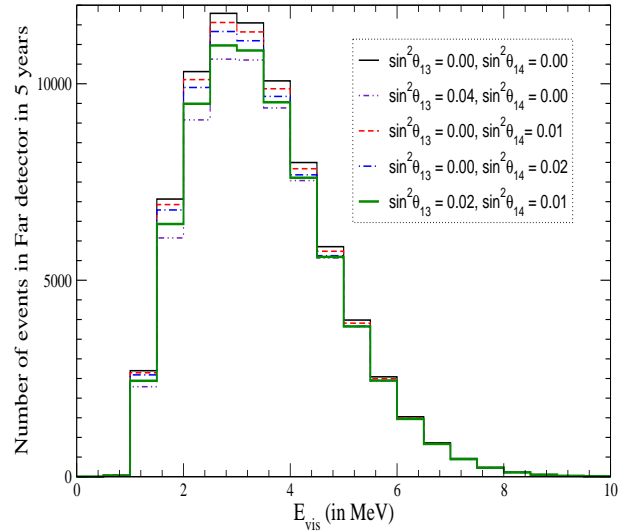
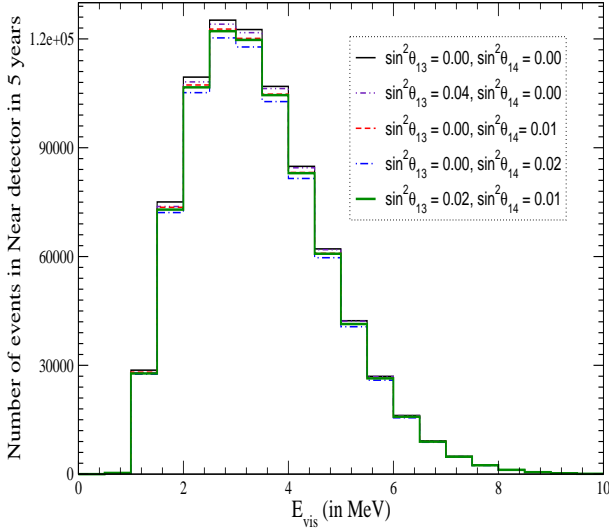


Figure 2: Number of events in 5 years expected at the near (left panel) and far (right panel) detectors of Double Chooz, as a function of the “visible energy” E_{vis} of the detected positron. The 5 different line types are for 5 combinations of $\sin^2 \theta_{13}$ and $\sin^2 \theta_{14}$ which are shown in the panels. We assume that $\sin^2 \theta_{15} = \sin^2 \theta_{14}$.

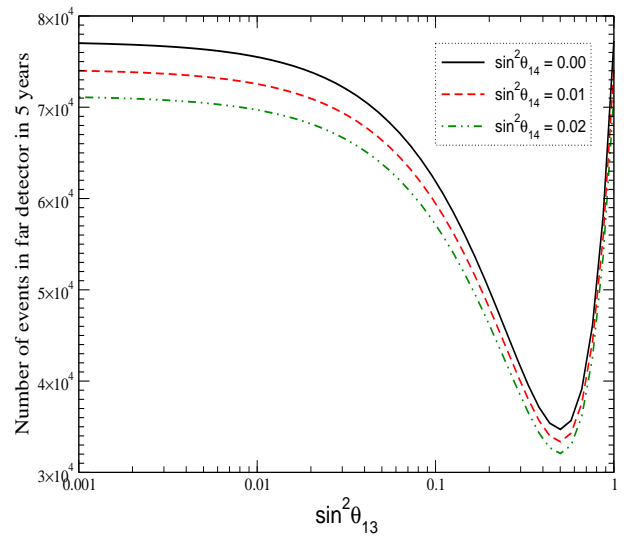
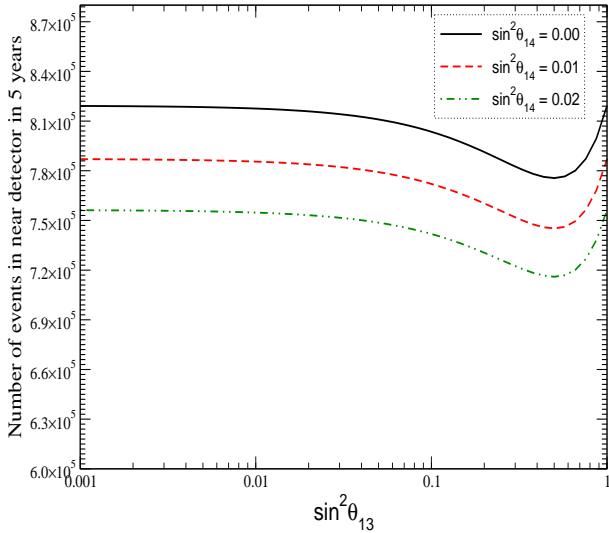


Figure 3: Total number of events in 5 years expected at the near (left panel) and far (right panel) detectors of Double Chooz, as a function of $\sin^2 \theta_{13}$. The black solid line is for $\sin^2 \theta_{14} = 0$, red dashed for $\sin^2 \theta_{14} = 0.01$ and green dot-dashed for $\sin^2 \theta_{14} = 0.02$. We assume that $\sin^2 \theta_{15} = \sin^2 \theta_{14}$.

We assume a second order polynomial parameterization of a_{ki} for the four isotopes ($i = {}^{235}\text{U}$, ${}^{239}\text{Pu}$, ${}^{241}\text{Pu}$, ${}^{238}\text{U}$). The coefficients are taken from Table 2 of [38]. The $\bar{\nu}_e$ are detected through their capture on protons

$$\bar{\nu}_e + p \rightarrow e^+ + n \quad (12)$$

whereby the e^+ and n give the prompt and delayed signal respectively in coincidence. The near and far detectors will be almost identical, consisting of a target volume of 10.32 m^3 of liquid scintillator comprising of 80% dodecane and 20% PXE, leading to 6.79×10^{29} free target protons. The scintillator is doped with 0.1% gadolinium. The computed number of positron events in n^{th} energy bin in the detector is given by

$$N_{N,F}^n = F_R \int_{E_n}^{E_{n+1}} dE_{vis} \int_0^\infty dE \sigma(E) R(E, E_{vis}) P_{\bar{e}\bar{e}}(E, L_{N,F}) \sum_i \frac{N_i^{fis} \phi_i(E)}{4\pi L_{N,F}^2}, \quad (13)$$

where E_{vis} is the measured *visible* energy of the emitted positron when the true visible energy $E_{vis}^T \simeq E - 0.8 \text{ MeV}$, with E being the energy of the incoming reactor antineutrino. The reaction cross-section is denoted by $\sigma(E)$ and $R(E, E_{vis})$ is the energy resolution function of the detector. The quantity F_R is given by

$$F_R = G \times P \times N_p \times T \times (1 - d_D) \times \epsilon_D, \quad (14)$$

where, G is the Global Load factor (reactor efficiency), P is the Reactor thermal power, N_p are the number of protons in the target volume, T is the exposure time, d_D is the dead time fraction of Detector D and ϵ_D is the detector efficiency. Values of all quantities needed for calculating the positron rate in the detector are taken from [12].

We show in Fig. 2 the number of events expected in 5 years as a function of the visible positron energy, for the near (left panel) and far detector (right panel). We show the event spectra for 5 different combinations of θ_{13} and θ_{14} (and θ_{15}) values. For the near detector it is mainly θ_{14} (and θ_{15}) values which cause difference to the event spectra. At the far detector oscillations with both frequencies are important and hence all the three mixing angles make a difference. We stress that even though we do not show the statistical errorbars on this figure for the sake of clarity, one can easily check that most of the cases of mixing parameters displayed on this figure should be statistically distinguishable by combining the near and far event spectra at Double Chooz.

In Fig. 3 we show the total observed positron events in 5 years as a function of $\sin^2 \theta_{13}$, for the near (left panel) and far detector (right panel). The three different line types in either of the panels show the results for a different choice for the value of θ_{14} (and θ_{15}). The net suppression of course increases as $\sin^2 \theta_{14}$ increases. This is true at both the near and far detectors. However, the $\sin^2 \theta_{13}$ dependence of the suppression is extremely mild at the near detector and very large at the far detector. As expected, the largest suppression comes at $\sin^2 \theta_{13} = 0.5$ at which we have maximal oscillations. The most important thing we can note from this figure is that for a certain range of events at the far detector, any given observed rate could be predicted by a wide set of possible values of θ_{13} and θ_{14} (and θ_{15}). All these would then constitute degenerate solutions. For instance, we can see from the figure that if the far detector was to observed 7×10^4 events in 5

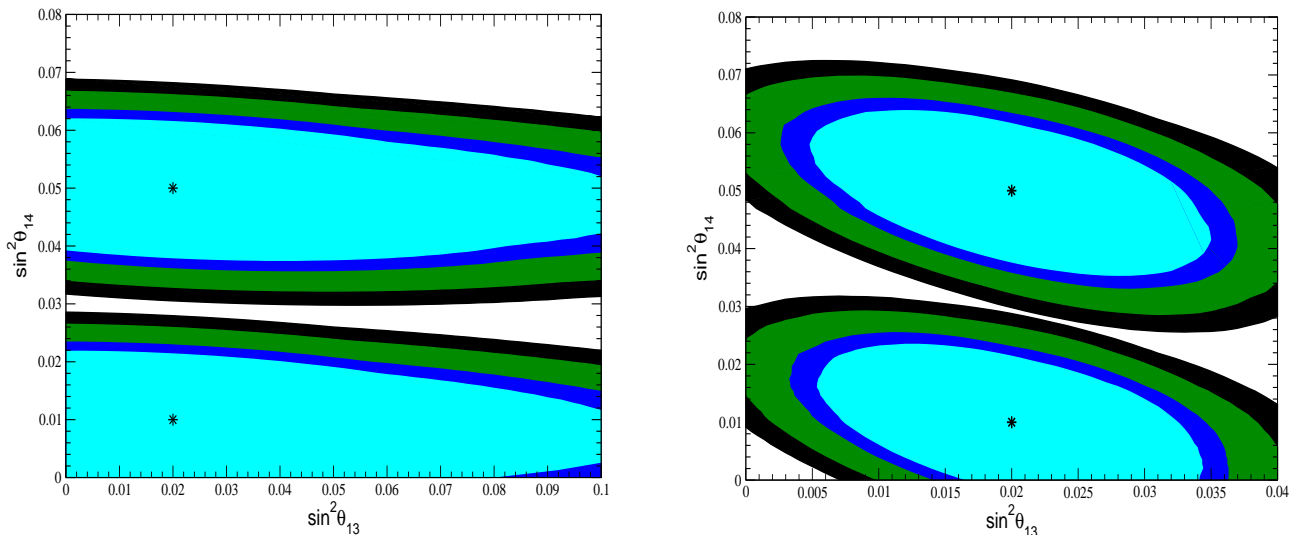


Figure 4: The 90%, 95%, 99% and 99.73% C.L. contours in the $\sin^2 \theta_{13} - \sin^2 \theta_{14}$ plane for different assumed true values of the mixing angles marked in the figure by stars. Left panel is for the data from near detector only while the right panel is for data from far detector alone. We assume that $\sin^2 \theta_{15} = \sin^2 \theta_{14}$.

years, then this would allow the sets of $(\theta_{13}, \theta_{14})$ values, $(0.043, 0.00)$, $(0.026, 0.01)$ and $(0.008, 0.02)$, as possible solutions. These would be degenerate solutions in this case. However, we can see by looking at the left panel that each of these combinations would predict different total rates at the near detector. Therefore by combining the near and far detected event rates, one can overcome this degeneracy problem.

3.2 The θ_{13} sensitivity

For estimating the projected sensitivity of the Double Chooz experiment to the mixing angles θ_{13} , θ_{14} and θ_{15} , we perform statistical analysis of 5 years prospective data at both the near and far detectors. We define a χ^2 function on the lines of [12]

$$\chi_R^2(\Theta_{true}) = \sum_{D=N,F} \sum_i \frac{[(1 + a_{corr} + a_{uncorr}^D + a_{spect}^i)N_D^i(\Theta_{fit}) - N_D^i(\Theta_{true})]^2}{N_D^i + B_D^i + (N_D^i \sigma_{bin})^2 + (B_D^i \sigma_{bkd})^2} + \frac{a_{corr}^2}{\sigma_{corr}^2} + \sum_{D=N,F} \frac{(a_{uncorr}^D)^2}{(\sigma_{uncorr})^2} + \sum_i \frac{(a_{spect}^i)^2}{(\sigma_{spect})^2}, \quad (15)$$

where D runs for the number of detectors (near and far) and i runs over the number of bins, Θ_{true} are the set of oscillation parameters at which the data is generated and Θ_{fit} is the corresponding set in theory. The systematic errors taken into account can be broadly characterized as normalization errors and spectral shape errors. The normalization errors include the 2% overall reactor antineutrino flux uncertainty which is relevant for both the detectors and therefore correlated. We denote this by σ_{corr} . The reminiscent uncorrelated normalization error between the detectors is

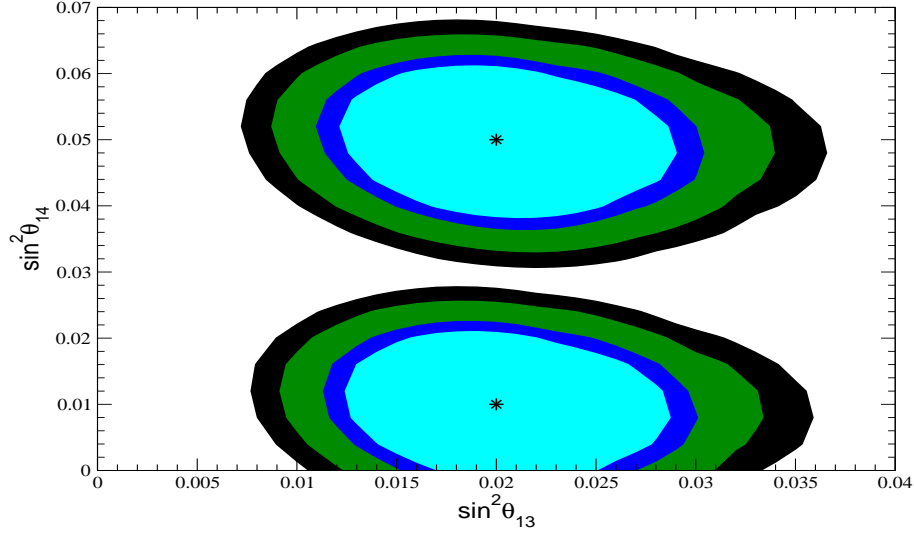


Figure 5: The 90%, 95%, 99% and 99.73% C.L. contours in the $\sin^2 \theta_{13} - \sin^2 \theta_{14}$ plane for assumed true values of the mixing angles marked in the figure by stars. Data from both near and far detectors are combined. We assume that $\sin^2 \theta_{15} = \sin^2 \theta_{14}$.

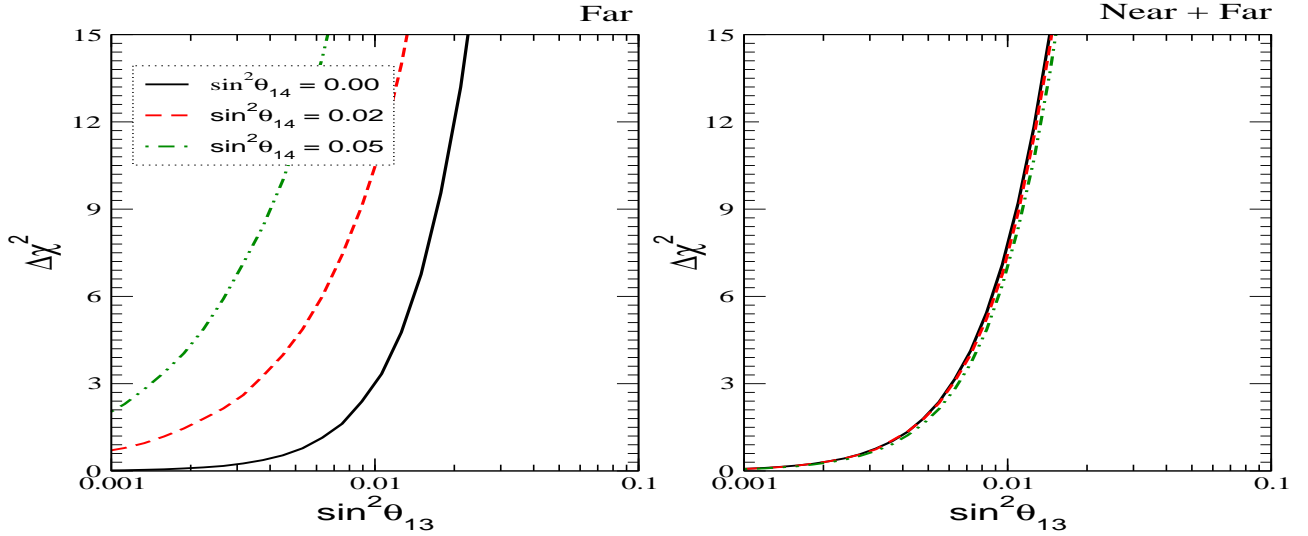


Figure 6: Sensitivity plot showing the $\Delta\chi^2$ as a function of $\sin^2 \theta_{13}$ for the far detector only (left panel) and when near and far data sets are combined (right panel). Data is generated at $\sin^2 \theta_{13} = 0$ and $\sin^2 \theta_{14} = 0$ for all curves in both panels. In the fit we fix $\sin^2 \theta_{14} = 0$ (black solid line), 0.02 (red dashed line) and 0.05 (green dot-dashed line). We assume that $\sin^2 \theta_{15} = \sin^2 \theta_{14}$.

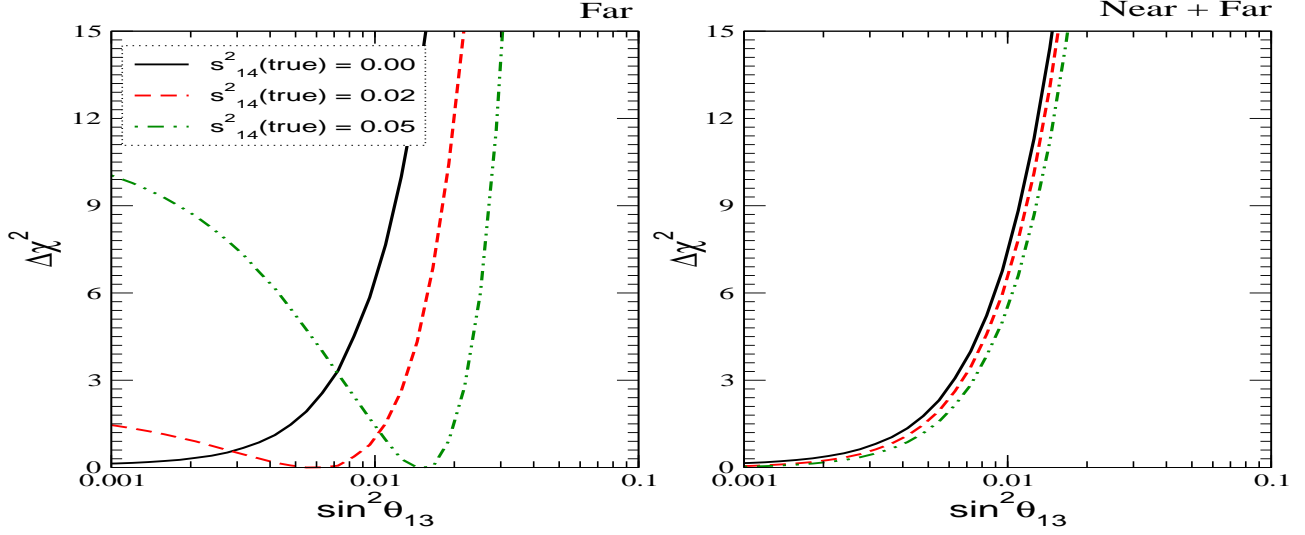


Figure 7: Sensitivity plot showing the $\Delta\chi^2$ as a function of $\sin^2\theta_{13}$ for the far detector only (left panel) and when near and far data sets are combined (right panel). Data is generated at $\sin^2\theta_{13} = 0$ and $\sin^2\theta_{14} = 0$ (black solid line) 0.02 (red dashed line) and 0.05 (green dot-dashed line). In the fit we fix $\sin^2\theta_{14} = 0$ for all curves. We assume that $\sin^2\theta_{15} = \sin^2\theta_{14}$.

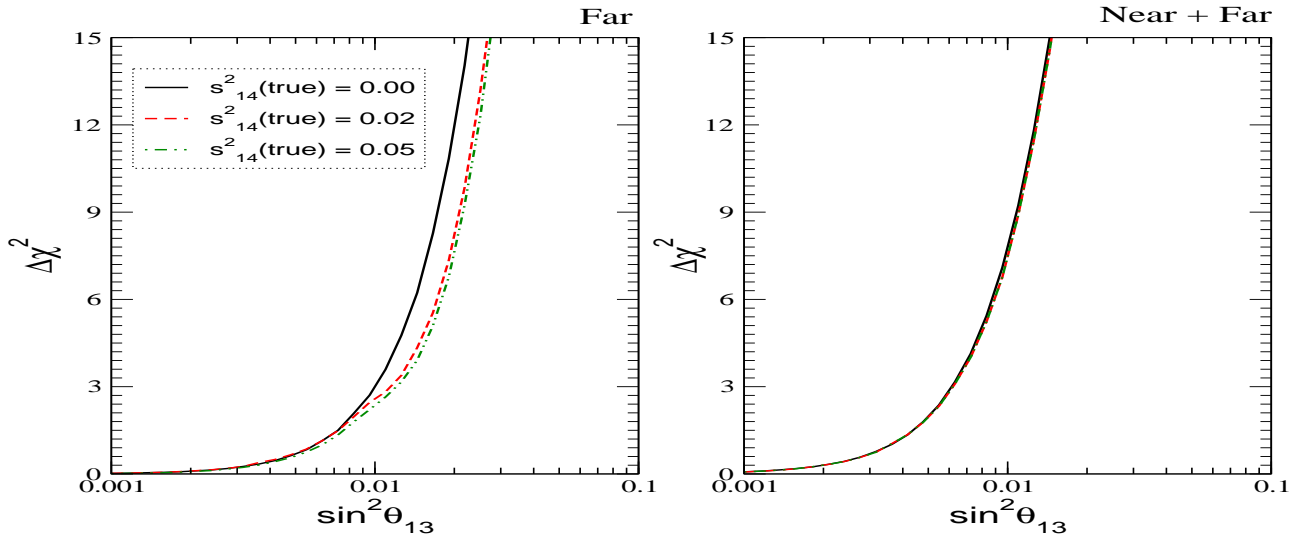


Figure 8: Sensitivity plot showing the $\Delta\chi^2$ as a function of $\sin^2\theta_{13}$ for the far detector only (left panel) and when near and far data sets are combined (right panel). Data is generated at $\sin^2\theta_{13} = 0$ and $\sin^2\theta_{14} = 0$ (black solid line) 0.02 (red dashed line) and 0.05 (green dot-dashed line). In the fit $\sin^2\theta_{14}$ is allowed to vary freely and take any possible value for all curves. We assume that $\sin^2\theta_{15} = \sin^2\theta_{14}$.

taken as 0.6% and is denoted as σ_{uncorr} . The uncertainty in the reactor $\bar{\nu}_e$ spectral flux is denoted by σ_{spect} and we take 2% as its estimated value. This error is totally uncorrelated between the near and far detectors. There is also a bin-to-bin uncorrelated systematic error which is denoted by σ_{bin} and taken as 1%. We also include the background subtraction error σ_{bkd} which is taken as 1% of the background, B_D^i , and we assume that there is 1% background. We have checked that the background and its corresponding error makes almost no difference to our final results. For each set of oscillation parameter value taken in the fit, the function $\chi_R^2(\Theta_{true})$ is minimized with respect to the parameters a_{corr} , a_{uncorr}^D and a_{spect}^i , which are allowed to vary freely.

In Eq. (15) we have explicitly put the subscript R on the χ^2 function to denote the contribution coming from the Double Chooz set-up alone. In our numerical analysis, we have also included a ‘‘prior’’ on the allowed values of Δm_{31}^2 since we expect that the uncertainty on this parameter will see some reduction by the time the Double Chooz results are declared. Our full χ^2 is therefore given by

$$\chi^2 = \chi_R^2 + \chi_{prior}^2, \quad (16)$$

where,

$$\chi_{prior}^2 = \left(\frac{\Delta m_{31}^2 - \Delta m_{31}^2(true)}{\sigma_{\Delta m_{31}^2}} \right)^2, \quad (17)$$

where we assume that $\Delta m_{31}^2(true) = 2.5 \times 10^{-3} \text{ eV}^2$ and $\sigma_{\Delta m_{31}^2}$ is 10% of $\Delta m_{31}^2(true)$. The total χ_{tot}^2 is then minimized with respect to some or all the oscillation parameters, to obtain the best-fit values, sensitivity limits and C.L. contours. In all our results presented in this paper, we marginalize over Δm_{31}^2 . We keep Δm_{21}^2 and $\sin^2 \theta_{12}$ fixed at their best-fit value due to reasons discussed before. For the mixing angles θ_{13} , θ_{14} and θ_{15} , we will always mention whether they are free or fixed in the fit.

In Fig. 4 we show the expected C.L. contours in the $\sin^2 \theta_{13} - \sin^2 \theta_{14}$ plane. The left panel shows contours expected from analysis of data from the near detector only, while right panel shows the corresponding results when only the far detector data is analyzed. The points at which the data were generated are shown by the ‘‘star’’ marks in the figure. The different color shades show the 90%, 95%, 99% and 99.73% contours. The $\Delta\chi^2$ for the C.L. contours correspond to 2 parameters. We see that the far detector can simultaneously constrain θ_{13} and the sterile mixing angles θ_{14} and θ_{15} . If the true value of $\sin^2 \theta_{13} = 0.02$ and $\sin^2 \theta_{14} = 0.05$, we could measure the sterile mixing angles within the range, $0.025 \leq \sin^2 \theta_{14} \leq 0.072$, at 3σ . If the true value was $\sin^2 \theta_{13} = 0.02$ and $\sin^2 \theta_{14} = 0.01$ the lower limit for $\sin^2 \theta_{14}$ would be restricted by 0 from below so that we would have $0.0 \leq \sin^2 \theta_{14} \leq 0.03$. For $\sin^2 \theta_{13}$ we see that at 95% C.L.⁴ $0.0026 \leq \sin^2 \theta_{13} \leq 0.037$ when data is at $\sin^2 \theta_{13} = 0.02$ and $\sin^2 \theta_{14} = 0.05$, and $0.003 \leq \sin^2 \theta_{13} \leq 0.036$ when data is at $\sin^2 \theta_{13} = 0.02$ and $\sin^2 \theta_{14} = 0.01$. We note from this that the limits on $\sin^2 \theta_{13}$ at the far detector depends on the value of $\sin^2 \theta_{14}$, albeit very slightly. Indeed the tilt of the C.L. contours towards the left shows a mild anticorrelation between the two mixing angles. We remind the reader that we keep $\sin^2 \theta_{15} = \sin^2 \theta_{14}$ fixed throughout this paper. The contours for the near

⁴We give the 95% C.L. for $\sin^2 \theta_{13}$ since above this the contours cross the y-axis.

detector explicitly show that there is hardly any sensitivity to $\sin^2 \theta_{13}$, unless its value was very large, which anyway is already disfavored. It could however restrict at 3σ the sterile mixing to $0.03 \leq \sin^2 \theta_{14} \leq 0.069$ if the true value was $\sin^2 \theta_{14} = 0.05$ and $0.0 \leq \sin^2 \theta_{14} \leq 0.028$ if the true value was $\sin^2 \theta_{14} = 0.01$. We see that the sterile mixing angle can be determined pretty well in either the near or far detector, with the precision in near detector being better due to its larger statistics.

In Fig. 5 we show the allowed areas at 90%, 95%, 99% and 99.73% C.L. for 2 parameter fit when data from near and far detector are combined using the full expression given by Eq. (15). For the case where the data was simulated at $\sin^2 \theta_{13} = 0.02$ and $\sin^2 \theta_{14} = 0.05$, the 3σ limits on the mixing angles are $0.007 \leq \sin^2 \theta_{13} \leq 0.037$ and $0.031 \leq \sin^2 \theta_{14} \leq 0.068$. For data at $\sin^2 \theta_{13} = 0.02$ and $\sin^2 \theta_{14} = 0.01$, corresponding limits are $0.008 \leq \sin^2 \theta_{13} \leq 0.036$ and $0.0 \leq \sin^2 \theta_{14} \leq 0.028$. We stress that we have given here the 3σ limits for $\sin^2 \theta_{13}$ while in the previous paragraph they were at the 95% C.L. Note that the sensitivity to $\sin^2 \theta_{13}$ improves dramatically. The reason of course is that the near-far detector combination effectively assures that the correlated systematic errors cancel out, leaving just the small uncorrelated part. The uncertainty on $\sin^2 \theta_{14}$ and $\sin^2 \theta_{15}$ is also somewhat reduced. Another significant feature we notice from the figure is that the near-far detector combination breaks the anticorrelation between $\sin^2 \theta_{13}$ and $\sin^2 \theta_{14}$ seen for the far detector in Fig. 4. The reason for this was discussed in the previous section.

If the true value of θ_{13} turns out to be very small or even zero then we would not see a positive signal at Double Chooz, at least in the three generation picture. We could nonetheless use the data to put an upper limit on the value of θ_{13} at a given C.L. In what follows, we will give the “ $\sin^2 \theta_{13}$ sensitivity reach” for Double Chooz. For this we generate the data at $\sin^2 \theta_{13} = 0$ and fit it back allowing for non-zero value for $\sin^2 \theta_{13}$. The resultant $\sin^2 \theta_{13}$ sensitivity reach is shown in Fig. 6, 7 and 8.

In Fig. 6 we have generated the data assuming the true values of $\sin^2 \theta_{13} = 0$ and $\sin^2 \theta_{14} = 0$ (and $\sin^2 \theta_{15} = 0$). We find the $\Delta\chi^2 = (\chi^2(\sin^2 \theta_{13}) - \chi^2_{min})$ for every value of $\sin^2 \theta_{13}$, keeping $\sin^2 \theta_{14}$ (and $\sin^2 \theta_{15}$) fixed at 0 (solid black line) 0.02 (red dashed line) and 0.05 (green dot-dashed line) in the fit. We note that the $\Delta\chi^2$ increases sharply with $\sin^2 \theta_{14}$ for the far detector alone. However, once we combine the data sets from near and far detectors, the effect of $\sin^2 \theta_{14}$ becomes very small. This is related to the fact discussed before that the combined near and far data sets are almost independent of the correlation between $\sin^2 \theta_{13}$ and $\sin^2 \theta_{14}$ and can measure both of them independently. In other words, the overall suppression or normalization factor due to $\sin^2 \theta_{14}$ gets canceled out from the fit for $\sin^2 \theta_{13}$, when data from the near detector is added to the data from the far detector.

In Fig. 7 we generate the data assuming the true value of $\sin^2 \theta_{13} = 0$ and taking $\sin^2 \theta_{14} = 0$ (black solid line), 0.02 (red dashed line) and 0.05 (green dot-dashed line). Here we find the $\Delta\chi^2$ for every value of $\sin^2 \theta_{13}$, keeping $\sin^2 \theta_{14}$ (and $\sin^2 \theta_{15}$) fixed at 0 in the fit for all cases. This situation might easily arise in practice if nature has indeed chosen a non-zero value for the sterile mixing angles and we being ignorant of that, try to fit the data by assuming that there were no sterile neutrinos mixed with the active ones. For the case where true value of $\sin^2 \theta_{14}$ was indeed 0, we have the standard three generation case and here we recover the projected $\sin^2 \theta_{13}$ sensitivity for Double Chooz. If only data from far detector was taken then we could put the limit $\sin^2 \theta_{13} < 0.0095$ ($\sin^2 2\theta_{13} < 0.038$) at 90% C.L. and $\sin^2 \theta_{13} < 0.017$ ($\sin^2 2\theta_{13} < 0.047$) at

3σ . For combined data from near and far detectors we could restrict the angle to $\sin^2 \theta_{13} < 0.006$ ($\sin^2 2\theta_{13} < 0.023$) at 90% C.L. and $\sin^2 \theta_{13} < 0.011$ ($\sin^2 2\theta_{13} < 0.043$) at 3σ . However, if the true value of $\sin^2 \theta_{14}$ was non-zero, we would have some difference in the sensitivity limit, if we were using data from the far detector alone. We would get a signal at the detector due to the sterile neutrinos and might confuse it with a signal due to $\sin^2 \theta_{13}$. It would look like we have observed a non-zero value of $\sin^2 \theta_{13}$. We note from Fig. 7 that the best-fit $\sin^2 \theta_{13}$ could be as large as $\sin^2 \theta_{13} = 0.012$ (0.027) if the true value of $\sin^2 \theta_{14}$ was 0.02 (0.05). This is the fake solution that we discussed about in the previous section. Once we combine the data sets from both near and far detectors, the impact of the sterile mixing angle is negated to a large extent. However, for very large values of $\sin^2 \theta_{14}$ such as 0.05, we find that some residual confusion and the fake solution remains. Also, the upper limit on $\sin^2 \theta_{13}$ at a given C.L. turns out to be different compared to the case where $\sin^2 \theta_{14}$ was indeed zero.

Fig. 8 is similar to Fig. 7 in most respect, except that here we allow $\sin^2 \theta_{14}$ (and $\sin^2 \theta_{15}$) to take all possible values in the fit. This would be the most democratic approach whereby all possible mixing angles are accounted for in the fit and marginalized over, while putting restrictions on θ_{13} . The effect of the sterile mixing angle on the allowed values of $\sin^2 \theta_{13}$ in this case is not dramatic. This is mainly due to the fact that $\sin^2 \theta_{14}$ and $\sin^2 \theta_{15}$ can now take non-zero values in the fit to give lowest possible χ^2 , while in Fig. 7 the only mixing angle we could fiddle with was $\sin^2 \theta_{13}$ since $\sin^2 \theta_{14}$ and $\sin^2 \theta_{15}$ were fixed at 0. When data at only the far detector is taken, the projected sensitivity on $\sin^2 \theta_{13}$ gets worse for true non-zero $\sin^2 \theta_{14}$, compared to when $\sin^2 \theta_{14}$ was truly zero in Nature. But once data from the near detector is added, the problem is solved and the standard projected sensitivity on $\sin^2 \theta_{13}$ is restored.

4 Conclusions

The recent MiniBooNE results, even though disagree with the LSND data, leave ample room for existence of extra sterile neutrinos. In particular, the 3+2 neutrino mass spectra with 2 extra sterile neutrinos mixed with the active ones can satisfy the world neutrino data if one allows for CP violation. In this paper we probed the implications of the 3+2 mass spectrum for the Double Chooz reactor experiment. We showed how the event spectra at the near and far detectors of the Double Chooz experiment change when we allow for sterile mixing. The oscillations driven by the extra sterile neutrinos would produce a constant suppression at both the near and far detectors of Double Chooz. This is in contrast to the Δm_{31}^2 driven and θ_{13} dependent oscillations which are almost absent in the near detector and only register their signal at the far detector. In the far detector, the extra oscillations due to sterile mixing would be superimposed over the normal flavor oscillation signal. In particular, we established that this sensitivity of the far detector to both θ_{13} and the sterile mixing angles leads to a correlation between the 2 completely different kinds of mixing angles.

We defined a χ^2 function for the statistical analysis of the data and presented our results. We showed that the presence of sterile mixing angles alter, albeit slightly, the precision with which θ_{13} could be determined in Double Chooz. The sterile mixing angle can be determined pretty well in either the near or far detector, with the precision in near detector being better due to

its larger statistics. The combined near and far detector data sets would be able to determine both mixing angles, though the precision in θ_{13} goes down as the true value of the sterile mixing angle increases. We also studied how the “sensitivity to $\sin^2 \theta_{13}$ ” changes in presence of sterile neutrinos. We defined the sensitivity reach as the maximum value of $\sin^2 \theta_{13}$ which would be able to fit the data at the chosen C.L., when its true value is exactly zero. If the true value of sterile mixing is indeed non-zero and we kept them fixed at zero in our fit, we would get significantly different results on the upper limit of $\sin^2 \theta_{13}$, even after combining the results from both near and far detectors. This problem would stay if we allowed the sterile mixing to vary freely in the fit, but analyzed results from the far detector only. We finally showed that the problem could be fully negated only by combining results from both detectors and allowing the sterile mixings to take all possible values in the fit.

In conclusion, presence of sterile neutrinos would leave its imprint on the signal at both the near and far detectors of the Double Chooz experiment. If only the far detector signal was considered, there is a possibility of confusing these sterile neutrino driven oscillations with active ones. However, by taking results from both detectors and allowing for the possibility of sterile mixing angles, one can probe both θ_{13} and the sterile mixing angles correctly at Double Chooz.

References

- [1] Y. Itow *et al.*, arXiv:hep-ex/0106019; D. S. Ayres *et al.* [NOvA Collaboration], arXiv:hep-ex/0503053.
- [2] P. Zucchelli, Phys. Lett. B **532**, 166 (2002); C. Volpe, J. Phys. G **34**, R1 (2007); S. K. Agarwalla, A. Raychaudhuri and A. Samanta, Phys. Lett. B **629**, 33 (2005); S. K. Agarwalla, S. Choubey and A. Raychaudhuri, Nucl. Phys. B **771**, 1 (2007); P. Huber, M. Lindner, M. Rolinec and W. Winter, Phys. Rev. D **73**, 053002 (2006); J. Burguet-Castell, D. Casper, E. Couce, J. J. Gomez-Cadenas and P. Hernandez, Nucl. Phys. B **725**, 306 (2005); J. Burguet-Castell, D. Casper, J. J. Gomez-Cadenas, P. Hernandez and F. Sanchez, Nucl. Phys. B **695**, 217 (2004); A. Donini, E. Fernandez-Martinez, P. Migliozzi, S. Rigolin, L. Scotto Lavina, T. Tabarelli de Fatis and F. Terranova, Eur. Phys. J. C **48**, 787 (2006); A. Donini and E. Fernandez-Martinez, Phys. Lett. B **641**, 432 (2006).
- [3] C. Albright *et al.* [Neutrino Factory/Muon Collider Collaboration], arXiv:physics/0411123 and references therein.
- [4] J. Burguet-Castell, M. B. Gavela, J. J. Gomez-Cadenas, P. Hernandez and O. Mena, Nucl. Phys. B **608**, 301 (2001).
- [5] H. Minakata and H. Nunokawa, JHEP **0110**, 001 (2001).
- [6] G. L. Fogli and E. Lisi, Phys. Rev. D **54**, 3667 (1996).
- [7] V. Barger, D. Marfatia and K. Whisnant, Phys. Rev. D **65**, 073023 (2002).

- [8] A. S. Dighe and A. Y. Smirnov, Phys. Rev. D **62**, 033007 (2000); C. Lunardini and A. Y. Smirnov, JCAP **0306**, 009 (2003); C. Lunardini and A. Y. Smirnov, Nucl. Phys. B **616**, 307 (2001); S. Choubey, D. Majumdar and K. Kar, J. Phys. G **25**, 1001 (1999); G. Dutta, D. Indumathi, M. V. Murthy and G. Rajasekaran, Phys. Rev. D **61**, 013009 (2000); A. S. Dighe, M. Kachelriess, G. G. Raffelt and R. Tomas, JCAP **0401**, 004 (2004); H. Minakata, H. Nunokawa, R. Tomas and J. W. F. Valle, Phys. Lett. B **542**, 239 (2002). A. S. Dighe, M. T. Keil and G. G. Raffelt, JCAP **0306**, 006 (2003); A. Bandyopadhyay, S. Choubey, S. Goswami and K. Kar, arXiv:hep-ph/0312315; T. Marrodan Undagoitia *et al.* J. Phys. Conf. Ser. **39**, 287 (2006); A. S. Dighe, M. T. Keil and G. G. Raffelt, JCAP **0306**, 005 (2003).
- [9] S. Choubey, N. P. Harries, and G. G. Ross Phys. Rev. D **74**, 053010 (2006). S. Choubey, N. P. Harries and G. G. Ross, arXiv:hep-ph/0703092.
- [10] K. Anderson *et al.*, arXiv:hep-ex/0402041.
- [11] F. Ardellier *et al.*, arXiv:hep-ex/0405032.
- [12] F. Ardellier *et al.* [Double Chooz Collaboration], arXiv:hep-ex/0606025.
- [13] J. C. Anjos *et al.*, Nucl. Phys. Proc. Suppl. **155**, 231 (2006).
- [14] X. Guo *et al.* [Daya Bay Collaboration], arXiv:hep-ex/0701029.
- [15] Information about the experiment available at <http://neutrino.snu.ac.kr/RENO>
- [16] V. Martemyanov, L. Mikaelyan, V. Sinev, V. Kopeikin and Yu. Kozlov, Phys. Atom. Nucl. **66**, 1934 (2003) [Yad. Fiz. **66**, 1982 (2003)]
- [17] Information about the experiment available at <http://mtheta13.uchicago.edu/>
- [18] M. Aoki *et al.*, arXiv:hep-ex/0607013.
- [19] L. Wolfenstein, Phys. Rev. D **17**, 2369 (1978);
- [20] S. P. Mikheev and A. Y. Smirnov, Sov. J. Nucl. Phys. **42**, 913 (1985) [Yad. Fiz. **42**, 1441 (1985)]; S. P. Mikheev and A. Y. Smirnov, Nuovo Cim. C **9**, 17 (1986).
- [21] V. D. Barger, K. Whisnant, S. Pakvasa and R. J. N. Phillips, Phys. Rev. D **22**, 2718 (1980)
- [22] S. K. Agarwalla, S. Choubey, S. Goswami and A. Raychaudhuri, Phys. Rev. D **75**, 097302 (2007).
- [23] A. A. Aguilar-Arevalo *et al.* [The MiniBooNE Collaboration], arXiv:0704.1500.
- [24] C. Athanassopoulos *et al.*, (The LSND Collaboration) Phys. Rev. Lett. **77**, 3082 (1996); C. Athanassopoulos *et al.*, (The LSND Collaboration) Phys. Rev. Lett. **81**, 1774 (1998).

- [25] J. J. Gomez-Cadenas and M. C. Gonzalez-Garcia, *Z. Phys. C* **71**, 443 (1996); S. Goswami, *Phys. Rev. D* **55**, 2931 (1997). S. M. Bilenky, C. Giunti and W. Grimus, *Eur. Phys. J. C* **1**, 247 (1998).
- [26] Y. Declais *et al.*, *Phys. Lett. B* **338**, 383 (1994); F. Dydak *et al.*, *Phys. Lett. B* **134**, 281 (1984); I. E. Stockdale *et al.*, *Phys. Rev. Lett.* **52**, 1384 (1984); B. Armbruster *et al.* [KARMEN Collaboration], *Phys. Rev. D* **65**, 112001 (2002); P. Astier *et al.* [NOMAD Collaboration], *Phys. Lett. B* **570**, 19 (2003).
- [27] M. Sorel, J. M. Conrad and M. H. Shaevitz, *Phys. Rev. D* **70**, 073004 (2004).
- [28] S. Goswami and W. Rodejohann, arXiv:0706.1462 [hep-ph].
- [29] M. Maltoni and T. Schwetz, arXiv:0705.0107 [hep-ph].
- [30] M. C. Gonzalez-Garcia and M. Maltoni, arXiv:0704.1800 [hep-ph]. M. Maltoni, T. Schwetz, M. A. Tortola and J. W. F. Valle, *New J. Phys.* **6**, 122 (2004), hep-ph/0405172; S. Choubey, *Phys. Atom. Nucl.* **69**, 1930 (2006); S. Goswami, *Int. J. Mod. Phys. A* **21**, 1901 (2006); S. Goswami, A. Bandyopadhyay and S. Choubey, *Nucl. Phys. Proc. Suppl.* **143**, 121 (2005); A. Bandyopadhyay, S. Choubey, S. Goswami, S. T. Petcov and D. P. Roy, *Phys. Lett. B* **608**, 115 (2005); G. L. Fogli, E. Lisi, A. Marrone and A. Palazzo, *Prog. Part. Nucl. Phys.* **57**, 742 (2006).
- [31] B. T. Cleveland *et al.*, *Astrophys. J.* **496**, 505 (1998); J. N. Abdurashitov *et al.* [SAGE Collaboration], *J. Exp. Theor. Phys.* **95**, 181 (2002) [*Zh. Eksp. Teor. Fiz.* **122**, 211 (2002)]; W. Hampel *et al.* [GALLEX Collaboration], *Phys. Lett. B* **447**, 127 (1999); S. Fukuda *et al.* [Super-Kamiokande Collaboration], *Phys. Lett. B* **539**, 179 (2002); B. Aharmim *et al.* [SNO Collaboration], *Phys. Rev. C* **72**, 055502 (2005).
- [32] Y. Ashie *et al.* [Super-Kamiokande Collaboration], *Phys. Rev. D* **71**, 112005 (2005).
- [33] E. Aliu *et al.* [K2K Collaboration], *Phys. Rev. Lett.* **94**, 081802 (2005).
- [34] D. G. Michael *et al.*, [MINOS Collaboration], arXiv:hep-ex/0607088.
- [35] T. Araki *et al.* [KamLAND Collaboration], *Phys. Rev. Lett.* **94**, 081801 (2005).
- [36] M. Apollonio *et al.*, *Eur. Phys. J. C* **27**, 331 (2003).
- [37] C. Bemporad, G. Gratta and P. Vogel, *Rev. Mod. Phys.* **74**, 297 (2002).
- [38] P. Huber and T. Schwetz, *Phys. Rev. D* **70**, 053011 (2004).